

See discussions, stats, and author profiles for this publication at: <https://www.researchgate.net/publication/271196796>

# Ionothermal Stability of Mesoporous Silica Films

ARTICLE *in* INDUSTRIAL & ENGINEERING CHEMISTRY RESEARCH · JANUARY 2015

Impact Factor: 2.59 · DOI: 10.1021/ie5041308

---

READS

24

2 AUTHORS, INCLUDING:



Jacob Prosser

UOP - Honeywell

8 PUBLICATIONS 84 CITATIONS

SEE PROFILE

# Ionothermal Stability of Mesoporous Silica Films

Jacob H. Prosser and Daeyeon Lee\*

Department of Chemical and Biomolecular Engineering, School of Engineering and Applied Science, University of Pennsylvania, Philadelphia, Pennsylvania 19104, United States

## Supporting Information

**ABSTRACT:** We have examined the ionothermal stability of mesoporous silica films (MSFs) in four different imidazolium ionic liquids (ILs) and compared it to their hydrothermal stability in liquid water. Ionothermal treatment of MSFs in anhydrous 1-butyl-3-methylimidazolium acetate, bromide, chloride, and thiocyanate reveals that MSFs are thermochemically stable in these ILs up to 175 °C for 24 h. Solvothermal stability of MSFs in imidazolium IL–water compositional mixtures was also investigated, and mesoporous silica is found to be stable in compositions greater than 25 mol % IL. A kinetic acceleration in MSF dissolution occurs at suitably low IL compositions relative to water for all ILs used and depends on the IL anion. Our findings suggest that anhydrous imidazolium ILs are unable to solvolytically depolymerize mesoporous silica, possibly making these better solvents than water for use with mesoporous silica.

## 1.0. INTRODUCTION

Mesoporous silica, typically synthesized by polycondensation of silicate species in the presence of pore templating materials (e.g., surfactants),<sup>1–5</sup> has found numerous applications in catalysis,<sup>6</sup> chemical sensing<sup>7</sup> and separations,<sup>8,9</sup> optics,<sup>10</sup> and thermal insulation<sup>11</sup> because of its high surface area, porosity, and tunable pore morphology and sizes. In particular, mesoporous silica is a very useful material for catalysis and separations because of its high thermal and mechanical stability,<sup>12</sup> wide ranging physical and surface chemical properties,<sup>13–17</sup> and relatively inexpensive and well-understood synthesis.<sup>18,19</sup> However, mesoporous silica can degrade in water even at room temperature, rendering its use in certain aqueous phase heterogeneous catalysis and separation applications impractical.<sup>20–23</sup>

Ionic liquids (ILs), also known as molten salts, have recently emerged as novel solvents for many different applications, particularly catalysis and separations, because of their chemical diversity, reputed thermochemical stability, and negligible vapor pressure, possibly serving as alternatives to aqueous solvents in applications with mesoporous silica.<sup>24,25</sup> One such promising example is the use of ILs instead of water as solvents for the catalytic depolymerization of lignocellulosic biomass.<sup>26–29</sup> Solid acids based on mesoporous silica could potentially serve as the catalyst in such IL-based biomass conversion processes.<sup>30–32</sup> Likewise, mesoporous silica materials infiltrated with ILs have been used as supported liquid phases for the separation of various compounds as well.<sup>33,34</sup> In order for these applications of porous silicas with ILs to be feasible, mesoporous silica must maintain its structure and properties in ILs under the range of conditions to which they are subjected. However, the ionothermal (i.e., in an anhydrous IL phase at temperatures higher than room temperature) stability of silica-based materials has not been studied rigorously. Only preliminary examinations of the ionothermal stability of certain macroreticulated organic resins and zeolites in imidazolium-based ILs have been conducted.<sup>28,35–37</sup> These studies found that organic resins dissolve in imidazolium ILs with certain anions, whereas

zeolites were chemically compatible with all IL phases and temperatures tested. We therefore believe that it is imperative to more rigorously examine the solvothermal (i.e., in a solvent at temperatures higher than room temperature) stability of mesoporous silica in ILs which to the best of our knowledge has yet to be reported.

We present our investigation of the solvothermal stability of supported mesoporous silica films (MSFs) in water, four different imidazolium ILs, and compositional mixtures of water and these ILs for the purpose of identifying their chemical suitability for use with one another at elevated temperatures. Imidazolium-based-ILs are selected because of their possibility of serving as solvent media for lignocellulosic biomass conversion processes, as well as their applications in separations.<sup>38–40</sup> Our choice of supported MSFs is because these allow for precise handling of mesoporous silica at small solid-to-solvent ratios and easier characterization by thin-film analysis techniques. We find that MSFs are indeed thermochemically stable in anhydrous imidazolium-based ILs, but their stability depends on the amount of water present. Furthermore, we discuss the possible mechanisms of MSF stability in the solvents we consider.

## 2.0. EXPERIMENTAL SECTION

A brief summary of our materials and methods is included in this section. For complete experimental details, please see the Supporting Information.

**2.1. Materials.** 1-butyl-3-methylimidazolium acetate (BMIM-AcO, ~97.0%, Figure 1a), 1-butyl-3-methylimidazolium bromide (BMIM-Br, ~99.9%, Figure 1b), 1-butyl-3-methylimidazolium chloride (BMIM-Cl, ~99.6%, Figure 1c), 1-butyl-3-methylimidazolium thiocyanate (BMIM-SCN, ~98.4%, Figure 1d), and tetraethylorthosilicate (TEOS,

**Received:** October 19, 2014

**Revised:** December 21, 2014

**Accepted:** January 5, 2015

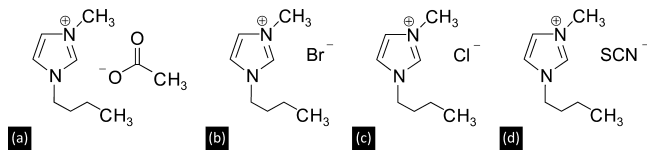


**Figure 1.** 2-D molecular structures of (a) BMIM-AcO, (b) BMIM-Br, (c) BMIM-Cl, and (d) BMIM-SCN. For each of the ILs depicted, the cation is the same (BMIM) while the anion varies as indicated.

~100.0%) were all purchased from Sigma-Aldrich and used as received. Pluronic F-127 ( $\text{PEO}_{106}\text{PPO}_{70}\text{PEO}_{106}$ , ~100.0%) was obtained from BASF and used without further treatment. All other chemicals and reagents used were acquired from Fisher Scientific and used as received. ILs and TEOS were stored and mainly handled inside a nitrogen gas inerted, positive pressure glovebox to prevent and minimize exposure to moisture. MSFs were deposited onto single-polish sided  $\langle 100 \rangle$  silicon wafers bought from University Wafer.

**2.2. Mesoporous Silica Film Fabrication and Solvo-thermal Treatment Methods.** MSFs were fabricated by dip coating at room temperature within ambient lab atmosphere using a dip withdrawal rate of 100 mm/min. Dip coat deposited MSFs were allowed to age at room temperature overnight (~18 h) in covered polystyrene Petri dishes at laboratory conditions. Following room-temperature aging, the triblock copolymer template was removed from the MSFs and film structure stabilized by subjecting these to a high-temperature treatment/calcination process in stagnant air. Template extracted MSFs were stored in covered polystyrene Petri dishes at laboratory conditions until these were used for solvothermal treatments (STTs, i.e., subjection to a solvent phase at temperatures higher than room temperature).

STTs were conducted on film pieces having average sizes of about  $3 \times 11 \text{ mm}^2$  that were score-cracked and cut from larger pieces generated during the dip coating film deposition process. Film pieces were submerged within about 3 g of the respective solvent required to conduct each treatment at the elevated temperatures at which the STTs were performed. All STT mixtures (i.e., film pieces and solvent mixture) were directly contained within polytetrafluoroethylene (PTFE) acid digestion liners with amenable PTFE lids obtained from Parr Instrument Co. having a nominal internal volumetric capacity of 45 mL. For all hydrothermal treatments (HTTs, i.e., subjection to a liquid water phase at temperatures higher than room temperature) and hydronothermal treatments (HHTTs, i.e., subjection to an ionic liquid–water binary solvent phase at temperatures higher than room temperature), PTFE liners were placed inside a corresponding acid digestion vessel to ensure evaporated water remained contained, while all ionothermal treatments (ITTs, i.e., subjection to an anhydrous ionic liquid phase at temperatures higher than room temperature) were conducted within only the PTFE liners not installed within an acid digestion vessel. Heating of the treatment mixture was accomplished by placing the treatment mixture container into a Fisher Isotemp vacuum oven (Model 281A) which controlled the enclosure temperature to within  $\pm 2^\circ\text{C}$ . Following the elapsed treatment duration, treatment containers were quenched in ice for 15 min to adequately cool and significantly decrease the effects of the solvent on the film pieces. Once cooled to near room temperature, all treatment mixtures were further quenched by mixing with about 15 g of deionized water, swirled for about 1 min, and allowed to sit at ambient lab

conditions for about 30 min in the capped PTFE liner to allow for adequate dissolution of the solvent used for the particular treatment. The diluted solvent mixture was decanted and saved for chemical analysis, and the film piece was removed from the PTFE liner and rinsed with flowing deionized water for about 15 s prior to washing in about 150 mL of stagnant deionized water for 30 min. Two additional water washes were performed following the same procedure in which the film piece was removed from the previous deionized water-wash bath, rinsed for about 15 s with flowing deionized water, and then resubmerged in about 150 mL of fresh deionized water for about 30 min. After complete water washing, film pieces were rinsed one final time with flowing deionized water for about 15 s and dried using flowing nitrogen gas, and then finally stored within polystyrene Petri dishes until post-STT characterizations for each could be performed.

**2.3. Mesoporous Silica Film Characterization.** The thicknesses and refractive indices (RIs) of MSFs were measured using spectroscopic ellipsometry (SE) before and after high-temperature calcination to confirm porogen removal and before and after all STTs. All film thickness and RI measurements reported in this work were made using a J.A. Woolam  $\alpha$ -SE fixed incidence angle, multiwavelength SE instrument with the source incidence and detection angles set at  $70^\circ$  relative to normal incidence and an irradiation wavelength range of 380–900 nm. Spectrum fitting was done with a Cauchy film and silicon substrate with a native silicon oxide layer model for all films over the entire irradiation wavelength range.

Field emission-environmental scanning electron microscopy (FE-ESEM) images were captured using a FEI-600 Quanta high-vacuum, FE-ESEM instrument with a peripheral-lens Evanhardt-Thornley secondary electron detector. Samples were sputter coated with a Quorum plasma generating coater with an iridium conductive layer to prevent significant charging and for capturing optimal image resolution. Only when required, thickness measurements made using SE were confirmed from those obtained by cross-sectional FE-ESEM imaging.

Field emission-scanning transmission electron microscopy (FE-STEM) images were captured using a JEOL-7500F high-vacuum, high-resolution FE-SEM instrument with a transmitted electron detector. STEM images of all film pieces were obtained after standard scanning electron microscopy (SEM) imaging and by scrape detachment of the film from the silicon substrate using a standard straight scalpel blade, collecting the fragmented and released film pieces using a  $5 \mu\text{L}$  deionized water drop suspended from a micropipette, and dispensing this film fragment–water drop suspension onto a 200 mesh transmission electron microscopy (TEM) copper support grid having solely an adhesive carbon layer on one side supplied by Ted Pella, Inc.

X-ray scattering was performed using a Rigaku SmartLab high-resolution intelligent X-ray diffraction system to examine the film pore structure and structural evolution following solvothermal treatments. All measurements made were done using the reflectance mode of the small-angle X-ray scattering (r-SAXS) method for this instrument and because films were deposited onto silicon wafer pieces.

## 3.0. RESULTS

**3.1. Mesoporous Silica Films.** Our MSFs are fabricated using an evaporation-induced self-assembly (EISA), block copolymer micelle templated, silica sol–gel fabrication method

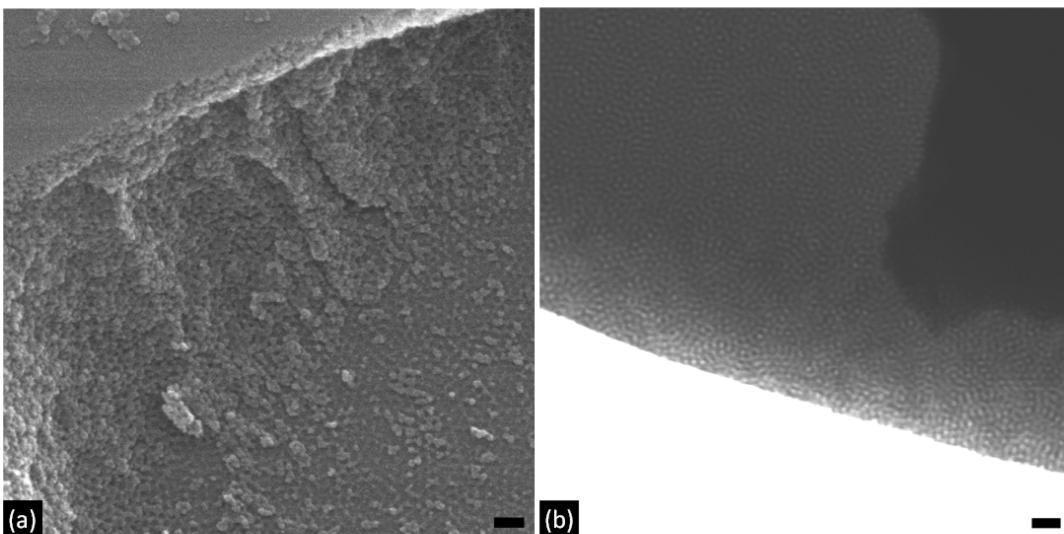


**Figure 2.** (a) Plan sectional view SEM image of an as-fabricated MSF taken at a spot where a partial cross-section can be seen; (b) STEM image of the same MSF as in (a). Scale bar lengths given in each image correspond to 50 nm.

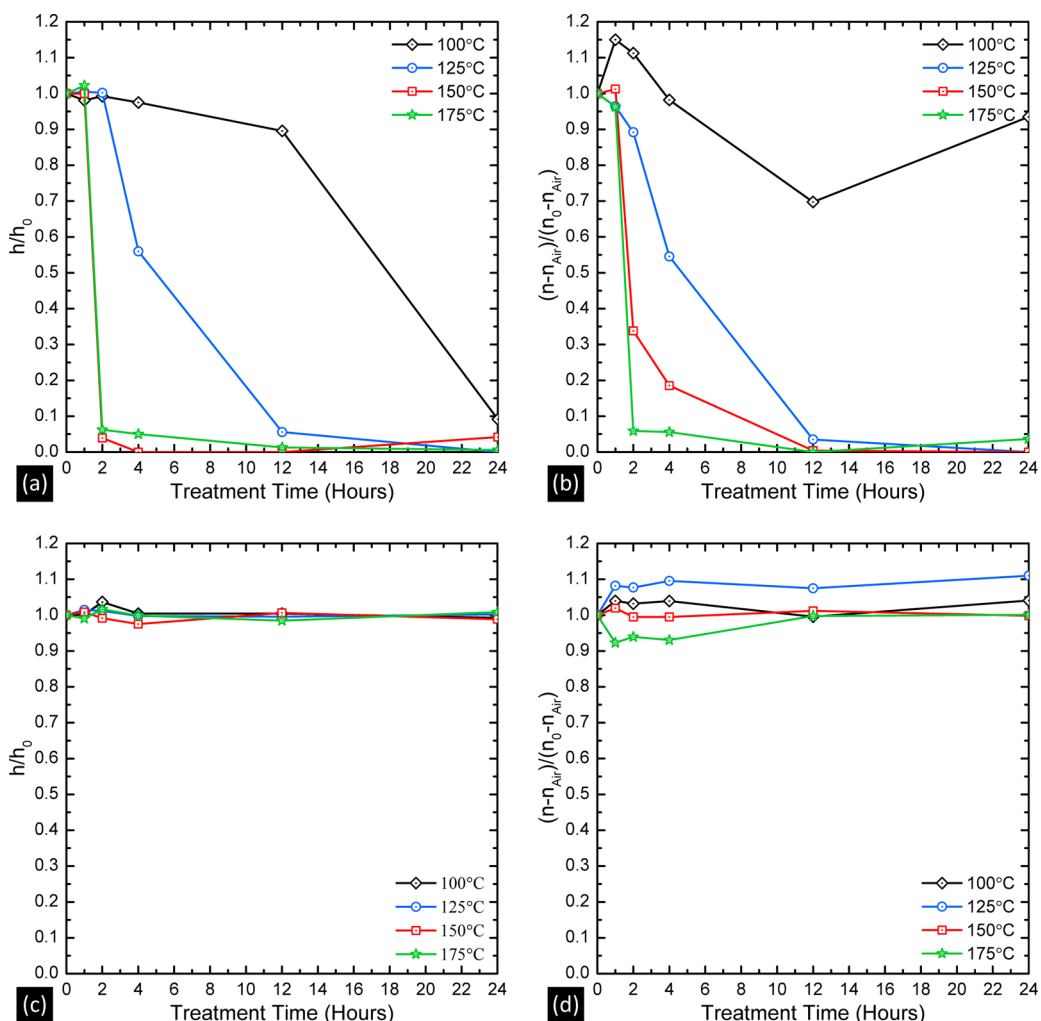


**Figure 3.** Plot of HTT-MSF (a) RFT and (b) RFRI, and ITT-MSF (c) RFT and (d) RFRI versus treatment time at various temperatures as measured by SE performed at ambient lab conditions. Trend lines provided are for direction along a specific data set and may not reflect the exact form of the dissolution profiles.

introduced and optimized by others.<sup>15,16</sup> Following this EISA sol-gel fabrication protocol, we reproducibly constructed about

150 nm thick MSFs having approximately 8–10 nm diameter cage-like, 3-D interconnected pores arranged in a hexagonally

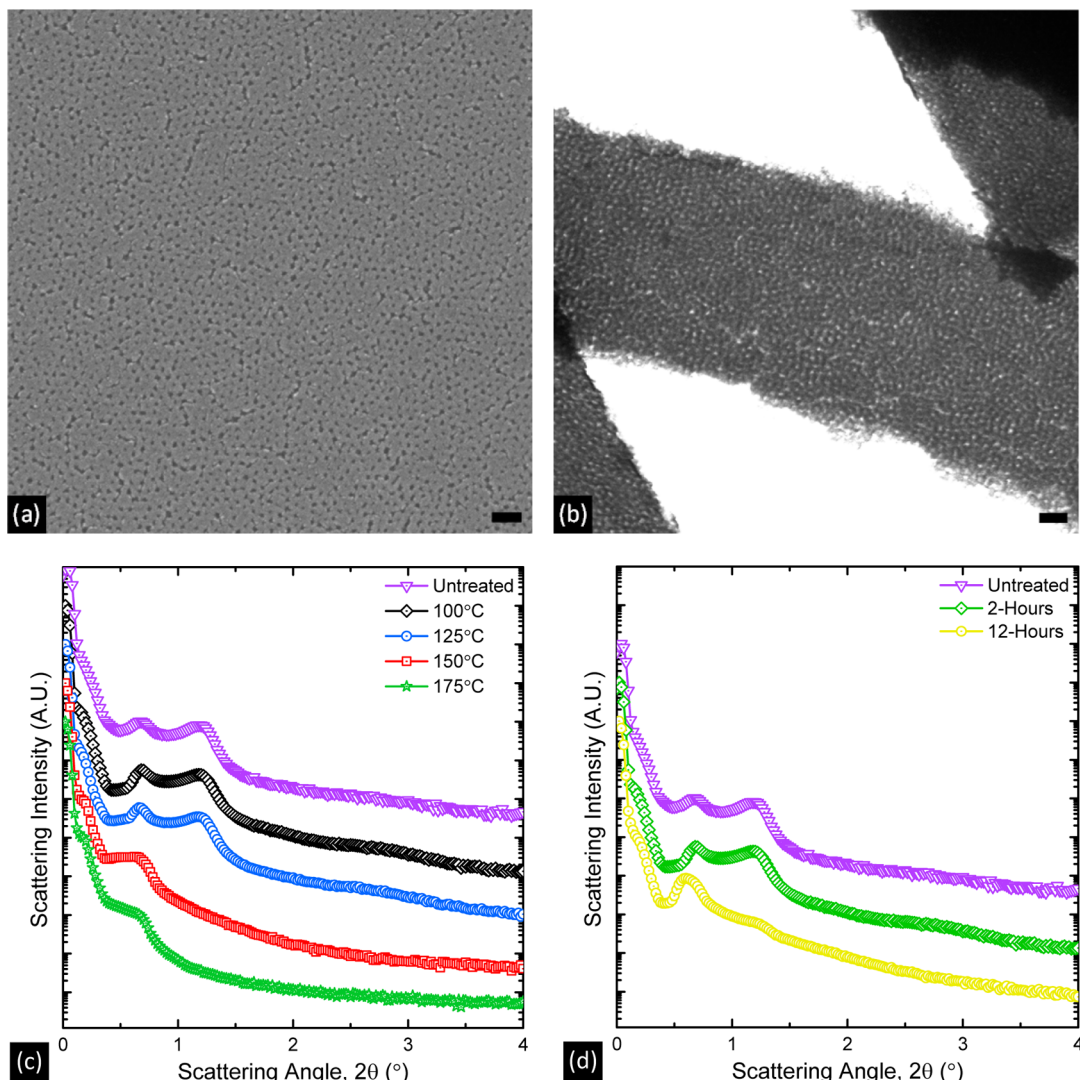


**Figure 4.** (a) Plan sectional view SEM image of a HTT-MSF treated at 100 °C for 12 h, taken of the exposed film–solvent interface resulting from hydrolytic dissolution by water; (b) STEM image of the same MSF as in (a); (c) plot of treated film r-SAXS profiles for HTT-MSFs treated for 2 h at various temperatures; and (d) plot of treated film r-SAXS profiles for HTT-MSFs treated for various times at 100 °C. Scale bar lengths given in each image correspond to 50 nm.

overlapping-pore network (Figure 2). Such a pore network was selected because of its common application as a support material in catalysis,<sup>41</sup> its relative ease of assembly and characterization,<sup>42</sup> and its interconnectivity.<sup>43</sup>

**3.2. Hydrothermal Treatment of Mesoporous Silica Films.** HTT of our MSFs in liquid water at certain temperatures in the range of 100–175 °C and over durations lasting greater than 1 h leads to a coincident decrease in the relative film thickness (RFT,  $\underline{h} = h/h_o$ , where  $\underline{h}$  is the RFT,  $h$  the treated film thickness, and  $h_o$  the initial, untreated film thickness)<sup>44–46</sup> (Figure 3a) and relative film refractive index (RFRI,  $\underline{n} = (n - n_{\text{Air}})/(n_o - n_{\text{Air}})$  where  $\underline{n}$  is the RFRI;  $n$  the treated film RI;  $n_o$  the initial, untreated film RI; and  $n_{\text{Air}}$  the RI of air) (Figure 3b). This temperature range was selected for our analysis because it spans the temperatures used by other researchers investigating the catalytic hydrolysis of cellulose in ILs.<sup>30–32</sup> The apparent decrease in the RFT and RFRI of HTT-MSFs is larger for higher treatment temperatures and for longer treatment times. Use of SEM, STEM, and r-SAXS confirms these results obtained by SE and that the film thickness decreases while the characteristic dimension and interconnec-

tivity of the pores increase, thereby explaining the drop in the film RI (Figure 4 and Supporting Information Figures S1 and S2). A decrease in the film thickness and increase in the characteristic pore size is represented in the r-SAXS scattering profiles by a subsequent decrease in the scattering intensity and left-shift of the singular diffuse reflectance peak situated at about a 1.20° 2-θ Bragg angle as both the HTT time and temperature are increased (Figure 4c,d).

**3.3. Ionothermal Treatment of Mesoporous Silica Films.** In contrast to the HTT of our MSFs, the ITT of the same type of MSF in either anhydrous BMIM-AcO (Figure 1a), BMIM-Br (Figure 1b), BMIM-Cl (Figure 1c), or BMIM-SCN (Figure 1d) does not cause a loss in either the RFT or RFRI even for the highest STT temperature (175 °C) and longest treatment duration (24 h) considered in this work (panels c and d in Figure 3, respectively, and Supporting Information Figures S6a,b, S7a,b, and S8a,b). Unchanging RFTs and RFRI of ITT-MSFs are likewise confirmed by examining their SEM, STEM, and r-SAXS measurements where the pore morphology appears to remain intact under varying treatment time, temperature, or IL anion type (Supporting Information Figures

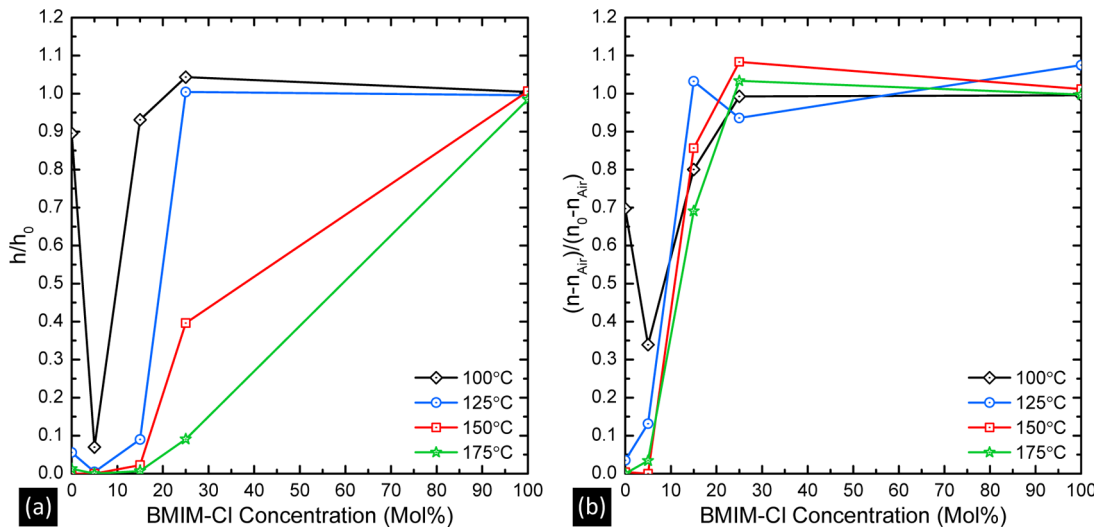


**Figure 5.** Plot of (a) RFT and (b) RFRI versus BMIM-Cl composition in water for HITT-MSFs treated for 12 h at various temperatures as measured by SE performed at ambient lab conditions. Trend lines provided are for direction along a specific data set and may not reflect the exact form of the dissolution profile.

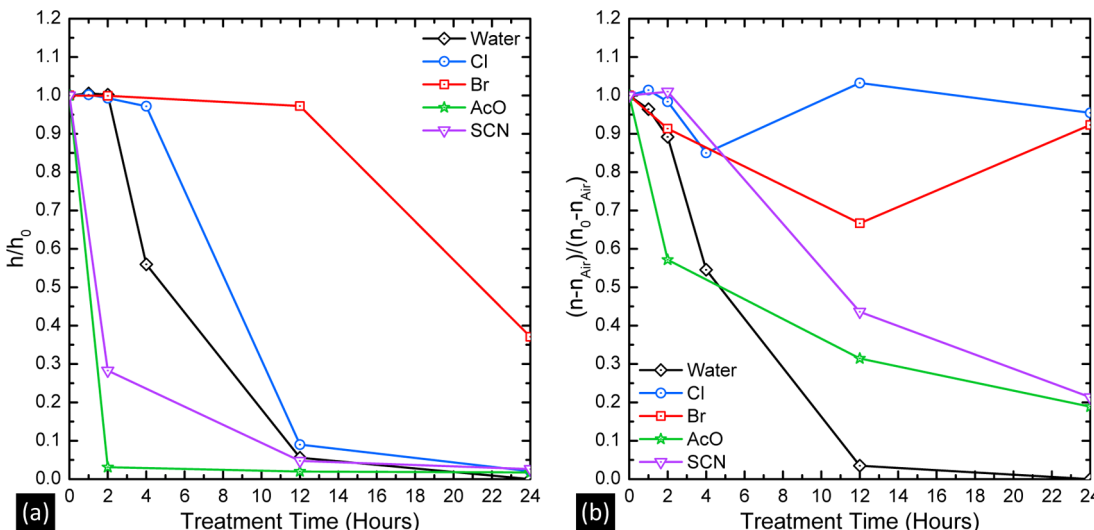


**Figure 6.** Plot of (a) RFT and (b) RFRI versus treatment time for HITT-MSFs treated in 15 mol % compositional mixtures of BMIM-AcO, BMIM-Br, BMIM-Cl, and BMIM-SCN ILs and water for 12 h at 125 °C as measured by SE performed at ambient lab conditions. Trend lines provided are for direction along a specific data set and may not reflect the exact form of the dissolution profile.

S3–S5 and S6c–h, S7c–h, and S8c–h). An increase in the RFRI seen for the 125 °C BMIM-Cl ITTs (Figure 3d) was discovered to be caused by residual organic material (possibly the IL itself) in the MSFs even after water washing. Upon oxygen plasma treatment we observe the RFRI to return to the initial film values while the thicknesses remain unchanged (see Supporting Information for plasma treatment details and Figure S27a,b).

**3.4. Hydronothermal Treatment of Mesoporous Silica Films.** During the HITT of our MSFs, for any given treatment time and temperature for any of the ILs used, we observe a decrease in both the RFT and RFRI when the IL composition is below about 25 mol % and essentially no change when the composition is some critical value greater than 25 mol % IL in water (Figure 5 and Supporting Information Figures S9 and S10). A HITT performed with a mixture composition of about 15 mol % BMIM-Cl in water surprisingly results in the same change in the RFT at nearly any temperature and change

in the RFRI at sufficiently high temperatures, as does a corresponding HTT performed at the same treatment conditions. Interestingly, these results suggest that the RFT and RFRI could have a maximum at some mixture composition between 0 mol % and 15 mol % BMIM-Cl.<sup>47–49</sup> In fact, a bulk acceleration in the rate of decrease of the HITT-MSF RFTs and RFIs is observed when the mixture composition is about 5 mol % BMIM-Cl. Such a behavior is most evident for lower temperatures at longer treatment times (Figure 5 and Supporting Information Figures S9c,d and S10c,d) whereas for higher treatment temperatures is more easily observed at shorter times (Supporting Information Figures S9a,b and S10a,b). Characterization of HITT-MSFs by r-SAXS confirms these results obtained through SE and that the pore structure is observed to disappear as both the treatment time and temperature are increased and the BMIM-Cl composition is some finite amount less than 25 mol % BMIM-Cl (Supporting Information Figure S11).

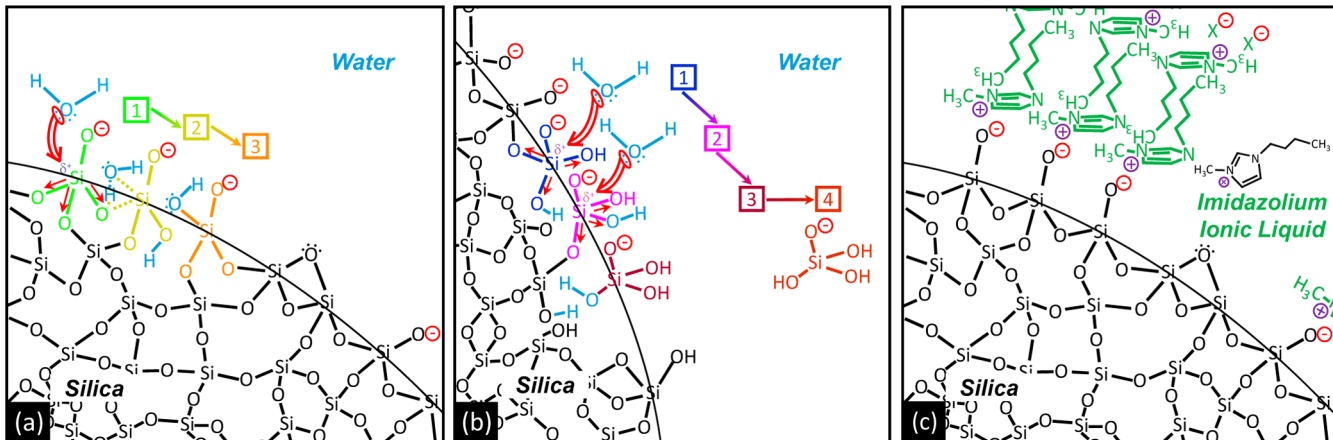


**Figure 7.** (a) Mechanism of a single silica surface hydrolysis reaction in water (steps 1, 2, and 3); (b) progression of successive silica surface hydrolysis reactions leading to dissolution and solubilization of orthosilicic acid (steps 1, 2, 3, and 4); and (c) possible structure formed at a silica/BMIM-IL or binary solvent mixture of a BMIM-IL and water having an appreciable IL composition. “X” denotes the IL anion which in this work could be  $X^- = \text{acetate} (\text{AcO}^-)$ ,  $\text{bromide} (\text{Br}^-)$ ,  $\text{chloride} (\text{Cl}^-)$ , or  $\text{thiocyanate} (\text{SCN}^-)$ . Pictorial elements contained in these illustrations are not to scale.

Additionally, when examining HITTs of our MSFs in BMIM-AcO, BMIM-Br, and BMIM-SCN we observe degradation behavior similar to that found for HITTs with BMIM-Cl. For some mixture composition less than 25 mol % of each IL in water, an acceleration in the bulk rate of decrease relative to pure water is evident in the RFT and RFRI plots of these HITT-MSFs for a given treatment time and temperature (Supporting Information Figures S13–S18). Apparent increase in the pore diameter and interconnectivity observed in both the SEM and STEM images for these HITT-MSFs is consistent with the SE results for HTTs (Figure 3a,b and Supporting Information Figure S12). The extent of degradation rate increase for a given solvent composition at the same treatment temperature is found to depend on the IL anion species. This IL anion dependence is explicit through a comparison of the RFT and RFRI versus treatment time for a given composition and treatment temperature between different ILs used (Figure 6 and Supporting Information Figures S19–S24). The overall rate of decrease in HITT-MSF RFTs and RFRI is found to increase for an IL anion ordering of  $\text{Br}^- < \text{Cl}^- < \text{SCN}^- < \text{AcO}^-$ .

## 4.0. DISCUSSION

**4.1. Hydrothermal Treatment of Mesoporous Silica Films.** MSFs are unstable in liquid water. Others determined that amorphous or crystalline, porous or nonporous, and thin film or free-particle forms of silica undergo degradation in liquid water by complete matrix depolymerization and dissolution.<sup>20,21,44</sup> The dissolution of silica in water can occur even at room temperature and neutral pH; however, this depends on many factors including the silica synthesis and processing conditions.<sup>44–46,50</sup> Chemical mechanisms hypothesized for silica dissolution by water is through a multistep pathway (Figure 7a). First, a direct hydrolysis depolymerization reaction occurs; interfacially solvating water molecules reversibly and heterolytically incorporate across the siloxane bridging bonds to form covalently and interfacially substituted silanols (Figure 7a, steps 1–3). Second, continued hydrolysis increases the degree of surface silanolization of partially hydrolyzed silica; upon sufficient hydrolysis of a tetrasubstituted silicon center, water-soluble silicic acid species are liberated (Figure 7b, steps 1–3). Lastly, released silicic acid

species are then homogeneously solvated and transported into the bulk aqueous phase (Figure 7b, step 4). Degradation by dissolution of our MSFs is similarly observed in liquid water, which is evident in the simultaneous decrease in the RFT and RFRI with increasing treatment time for any particular temperature (panels a and b of Figure 3, respectively). A decrease in the RFT indicates that the film is dissolving at the solid film–bulk liquid-phase interface, while a drop in the RFRI denotes internal dissolution of the film at the pore walls.<sup>44–46</sup> Internal dissolution is also confirmed by SEM, STEM, and r-SAXS measurements as the pores are observed to chain together and enlarge radially as treatment time is increased for a given treatment temperature (Figure 4a–d and Supporting Information Figures S1 and S2). The coincident change in the RFT and RFRI signifies isotropic dissolution throughout each MSF. Such dissolution uniformity is most logically due to the pore interconnectivity, complete solvent infiltration into the mesoporous network, a negligible mass-transfer resistance of dissolving silicate species within the film, and an insignificant boundary layer to mass transfer at the solid film–solvent interface.

Complete dissolution of our MSFs in water occurs for any given temperature over a long enough duration because we used approximately an order of magnitude ( $10\times$ ) in excess of the amount of water capable of dissolving at room temperature the quantity of silica contained in these MSFs.<sup>20,44–46,50</sup> Additionally, MSF dissolution during HTT accelerates as the treatment temperature is increased (Figure 3a,b). Because water is both the solvent and a reactant, temperature impacts both its solvating and kinetic reaction properties. Therefore, acceleration in the dissolution rate with increasing solution temperature implies intensification in (i) the driving force for dissolution, suggesting that silica behaves like a directly soluble salt and its dissolution is endothermic; and/or (ii) the kinetic rate of interfacial hydrolysis, indicating the overall and apparent activation energy is most likely positive, suggesting that there may be a rate-limiting step of the hydrolysis process. The severity of the thermal dependence of these factors then dictates how dissolution occurs in response to temperature.

Although the dissolution induced by the HTT of silica appears as though it is purely a dielectric mechanism such as for

the dissolution of an ionic salt like sodium chloride (NaCl) in water, in fact it relies on both the propagation of hydrolysis reactions and molecular dissolution through dielectric screening. Accordingly, it is minimally required for the solvent to contain chemical species, such as the solvent itself or a homogeneously dissolved solute having interfacial activity, that are capable of breaking the siloxane bonds so silica can molecularly dissolve.

#### 4.2. Ionothermal Treatment of Mesoporous Silica Films.

In contrast to the dissolution of mesoporous silica in liquid water, the degradation of our MSFs by this form in anhydrous BMIM-AcO<sup>-</sup>, -Br, -Cl, or -SCN ILs does not occur. The ionothermal stability of our MSFs is apparent in the time-invariant RFT, RFRI, SEM, STEM, and r-SAXS measurements for any given treatment temperature and all ILs used (Figure 3c,d and Supporting Information Figures S3–S8). Therefore, it is reasonable to conclude that MSFs are thermochemically compatible and stable within these ILs and that mesoporous silica does not ionothermally degrade.

Dissolution of our MSFs does not occur during ITTs likely because of (i) the inability of the anhydrous IL to covalently disrupt the silica network leading to depolymerization and/or (ii) the insolubility of formed monomeric or oligomeric silicate species in these ILs. IL cations are not able to induce silica depolymerization probably because steric hindrance of the bulky cation from covalently accessing the silica surface prevents cationic ionolysis. Additionally, because the cationic charge density is relatively low, its electrophilic substitution onto oxygen bridges is not likely. Therefore, any degradation leading to dissolution through homologous ion substitution causing siloxane breakage would most likely be from the highly charge-concentrated and less sterically hindered IL anion.

IL anions can break siloxane bridges only through their direct nucleophilic substitution onto a surface silicon atom. Nucleophilic attack by IL anions could occur and may depolymerize the silica network because the aqueous phase nucleophilic strengths of all IL anions considered here are greater than that of water. Additionally anion-induced depolymerizaton of silica in anhydrous IL could occur because silanes with many different types of coordination ligands exist, thus implying that the anions used in our study may be suitable to covalently coordinate silicon as ligands. Also, nucleophilic attack by the IL anion is possible given that the IL phase is a lower dielectric medium. But this process will only occur if there is no significant ionic structuring near the surface which will prevent strong anionic interaction with surface silicon atoms. Yet even with higher nucleophilicity in a lower dielectric medium, the IL anion still cannot adequately promote siloxane bond cleavage facilitating dissolution. This suggests that either significant ionic structuring does occur or the chemical nature of the nucleophilic substitution requires additional stabilization that the IL cannot impart. IL cation adsorption onto exposed silanols causing substantial surface coverage, which has been proposed previously,<sup>51,52</sup> is a specific example of ionic structuring that could chemically passivate the silica surface from nucleophilic attack and substitution by the IL anions (Figure 7c). Such a structure might impede the anion nucleophilic interaction with surface siloxane groups depending on the degree of cation surface coverage.

Alternatively, MSF disintegration in ILs may not occur as formed silicates may be insoluble in ILs and thus undergo immediate reprecipitation following depolymerization. However, such a futile process would produce a free energy

minimized silica structure that likely is different from the initial structure of our untreated MSFs. Because no restructuring within our MSFs is found following ITTs, as evidenced by SEM and r-SAXS, a dissolution–precipitation process is presumably not occurring. It is plausible to expect solubility of negatively charged silicates in ILs because many are known to promote long-range ionization and dissociation of certain salts due to their ability to preserve long-range charge neutrality.<sup>53</sup> Thus, negatively charged species formed from heterolytic cleavage of siloxane bonds could homogeneously dissolve in ILs. Although we do not fully understand the mechanism behind the thermochemical stability of MSFs in ILs, it is our hypothesis that MSF stability against dissolution in BMIM-based ILs is because of their preferential interfacial contact and the IL's inability to permanently react with the silica surface, either forming irreversible surface complexes or inducing interfacial ionolytic depolymerization leading to homogeneous dissolution.

#### 4.3. Hydronothermal Treatment of Mesoporous

**Silica Films.** Dissolution of our MSFs in binary IL–water solvent mixtures is also observed. We expect this instability because our MSFs dissolve in water, and water is present in most of these binary solvent mixtures in large quantities. Although, unexpectedly, we in fact find that the dissolution rate is maximum at a mixture composition between water and anhydrous IL. This is evident in the dissolution rate acceleration revealed at a low IL mixture composition (Figure 5 and Supporting Information Figures S9, S10, and S13–S18). Given that MSFs are found to dissolve in water but not in the ILs used, it is intuitive to presume that binary solvent mixtures of IL–water would yield MSF dissolution rates intermediate those in the two pure solvents and that a monotonically decreasing dissolution rate with increasing IL composition would be expected for MSFs during HITTs. However, because we observe a dissolution rate increase at appreciably small IL compositions, some unforeseen binary solvent nature is identified.

We explain this HITT dissolution enhancement similarly to how the temperature induced accelerations in HTT-MSFs are explained, where binary solvent compositional changes shift the (i) solubility driving force and/or (ii) kinetic rate of interfacial solvolysis. The extended Hildebrand solubility criteria, which identifies thermodynamic solvation qualities of nonregular solvents, supports that compositionally nonmonotonic MSF dissolution is from silicate solubility. Conversely, IL ion surface adsorption and participation in the interfacial solvolysis mechanism substantiates interfacial kinetics as the source for this dissolution behavior.

The extended Hildebrand solubility theory for nonregular binary solvent mixtures stipulates that dissolution enhancements can occur for solutes with Hildebrand solubility parameters between those of the pure solvents.<sup>54</sup> Additionally, the binary solvent composition that produces a maximum solute solubility has a solubility parameter equal to that of the solute's. Consequently, the solubility versus binary solvent composition profile varies continuously and according to the extended Hildebrand solubility requirements between the solubility maximum at some intermediate binary solvent composition and the pure solvent solubilities.

The bulk dissolution rate of a nonreacting solute in a dielectric solvent is directly proportional to the extent away from its solubility. Consequently, for a given solution concentration of a dissolving solute, the dissolution rate will

mirror the solubility concentration and how it varies with solution conditions. Therefore, the form of solubility versus binary solvent composition profile translates into that of the dissolution rate versus solvent composition profile.

Considering the ideal dissolution case in which silica is fully hydrolyzed to orthosilicic acid and dissolved homogeneously in this form, the respective solvent enhancement composition can be estimated using the Hildebrand solubility criteria. The Hildebrand solubility parameter for orthosilicic acid is in fact computed to be ( $\delta_{\text{Si(OH)}_4} = 46 \text{ (J/cm}^3)^{1/2}$ ), intermediate to those for water ( $\delta_{\text{H}_2\text{O}} = 48 \text{ (J/cm}^3)^{1/2}$ ) and for the ionic liquids ( $24 < \delta_{\text{BMIM-IL}} < 25 \text{ (J/cm}^3)^{1/2}$ ) used in this work. Using these values with the extended Hildebrand solubility criteria, a dissolution enhancement composition is estimated approximately at a BMIM-IL composition of ~1 mol % of IL (see Supporting Information for estimation details). This estimate is close to the acceleration composition observed (~5 mol %), suggesting that the HITT dissolution behavior of MSFs is possibly due to the solubility driving force and not the interfacial depolymerization mechanism.

Alternatively, we note that solvent composition effects on the interfacial solvolysis process could instead explain the observed dissolution phenomenon in IL–water mixtures. Because ILs are ionically dissociable, when mixed at low concentrations in a suitable solvent these behave as dissolved electrolytes.<sup>55,56</sup> In fact, because we used imidazolium ILs having cations with significantly hydrophobic chainlike substituent groups, these cations behave like cationic surfactants when dissolved in water due to their inherent amphiphilicity.<sup>57</sup> It is plausible then that the IL cation can preferentially adsorb from aqueous solution onto our MSFs, as found for other cationic surfactants in aqueous solution with metal oxide interfaces.<sup>58</sup> Moreover, aqueous solutions of 1:1 or 1:2 electrolyte mineral salts, such as sodium chloride (NaCl) or calcium chloride (CaCl<sub>2</sub>), respectively, dissolved at sufficiently low concentrations are known to enhance the dissolution of nonporous quartz<sup>59</sup> and amorphous silica.<sup>60</sup> These dissolution accelerations are attributed to an apparent increase in the interfacial nucleophilicity of water induced through electrophilic withdrawing from surface silanols by adsorbed salt cations. Once adsorbed at appropriately small concentrations, and hence surface coverages, the IL cation could electrophilically induce dissolution leading to a dissolution enhancement during HITTs (Figure 5 and Supporting Information Figures S13–S18).

Subsequently, for HITT compositions exceeding the enhancement composition, we observe a steady decrease in the dissolution rate to the minimum found in ITTs. This finding contradicts those with aqueous salt solutions, in which dissolution rates remain augmented for compositions even an order of magnitude higher than the enhancement composition.<sup>59,60</sup> Subsequent decrease following enhancement is reasonable if steric hindrance of water by cation surface shielding occurs. Formation of a densely covered cation adsorption layer may passivate the silica surface from nucleophilic attack by water, in turn decreasing the dissolution rate (Figure 7).<sup>50,61,62</sup> Passivation by cation adsorption is similar to the formation of self-assembled monolayers of ionic surfactants on surfaces, which, depending on their assembly, can modify and/or completely reverse the wettability of certain solid surfaces. Surface passivation at high IL cation compositions, and surface coverages, are consistent with enhancements found at low IL solution concentrations.

Therefore, an interfacial solvolysis mechanism involving cationic surface adsorption supports the observed HITT-MSF dissolution profiles.

**4.4. Ionic Liquid Anion Impact on Hydronothermal Treatment of Mesoporous Silica Films.** When we change the identity of the IL anion, we observe additional dissolution acceleration. This anionic-dependent dissolution acceleration is attributed to an increase in the interfacial solvolysis depolymerization process caused by IL anion (i) catalysis according to its aqueous phase nucleophilicity and ionic radius and/or (ii) hydrolysis of water producing hydroxide anions which directly act as interfacial nucleophilic catalysts boosting silica solvolysis rates according to the amount of hydroxide produced.

Nucleophilic interaction between the IL anion and a silica surface–silicon center due to the intrinsic silanol bond polarization or a polarization induced by tandem IL cation adsorption through ion exchange with surface silanols could weaken siloxane bonds making these more susceptible to nucleophilic attack and breakage by water. If anion nucleophilic interaction does occur, then MSF dissolution rates at low IL concentrations should be directly related to the anion aqueous phase nucleophilic strength. Consequently, a dissolution rate ordering of Cl<sup>−</sup> < Br<sup>−</sup> < OH<sup>−</sup> < SCN<sup>−</sup>, which follows the anion nucleophilicity, should be observed.<sup>63</sup> We hypothesize that hydroxide is formed when BMIM-AcO is dissolved in water because of the weakly basic nature of the acetate anion, as this is capable of hydrolyzing water to generate acetic acid (neutrally protonated acetate) and hydroxide, in turn raising the solution pH. Because the nucleophilicity and hydrated size of hydroxide are substantially larger and smaller, respectively, than those of the acetate anion, hydroxide should then dominate in the nucleophilic attack on any electrophilic nodes in solution. Therefore, we believe that in the case of BMIM-AcO–water mixtures, hydroxide is formed and this is the anion predominantly leading to the nucleophilic catalyzed depolymerization of our MSFs. However, the observed anion ordering, Br<sup>−</sup> < Cl<sup>−</sup> < SCN<sup>−</sup> < OH<sup>−</sup>, (Figure 6 and Supporting Information Figures S19–S24) is inverted with respect to the two anion nucleophilic classes (i.e., Cl<sup>−</sup> and Br<sup>−</sup> as group VII, and OH<sup>−</sup> and SCN<sup>−</sup> as group VI and V). This nucleophilic inversion could be from IL ion coadsorption (i.e., both cation and anion adsorb onto the surface). Coadsorption may sterically hinder IL anion access to the silica surface because of the bulkiness of the imidazolium cation. Steric hindrance caused by coadsorption will therefore depend on the anion size and is expected only for sufficiently high IL cation surface coverages. Effective anion radii are known to increase as OH<sup>−</sup> < Cl<sup>−</sup> < Br<sup>−</sup> < SCN<sup>−</sup>.<sup>64</sup> Considering now the relative anion size, for if anion steric hindrance by surface adsorbed cations occurs, the anticipated dissolution rate ordering could then follow that found experimentally (Br<sup>−</sup> < Cl<sup>−</sup> < SCN<sup>−</sup> < OH<sup>−</sup>). This then qualitatively suggests that HITT-MSF dissolution is from solvent phase influences on the interfacial solvolysis rate. Steric hindrance of the IL anion due to coadsorption with high cation surface coverages is consistent with the dissolution enhancement found at suitably low IL compositions. Therefore, anionic-dependent dissolution behavior at sufficiently large HITT-IL compositions is further evidence supporting an IL interfacial adsorption dissolution mechanism, thus controlling the overall dissolution kinetics.

We also find that solution pHs of HITT solvent mixtures for any solvent composition increase by the same anion ordering

( $\text{Br}^- < \text{Cl}^- < \text{SCN}^- < \text{AcO}^-$ ) as the dissolution rates (Supporting Information Figure S26). HITT mixture pHs may differ for different IL anions in water because of their acid/base nature as these can either protonate or hydrolyze water resulting in a different mixture pH. Likewise, deprotonation of the imidazolium cation at the C2-position forming a reactive carbene has been detected and can simultaneously lower the pH.<sup>65,66</sup> Silica dissolution rates in water are known to increase with increasing hydroxide concentration as it is hypothesized that hydroxide catalyzes the interfacial hydrolysis of silica.<sup>20,21,67–69</sup> Because HITT-MSF dissolution rates correspond to solution pHs, it is reasonable to infer that hydroxide anions formed from the hydrolysis of water by IL anions accelerate the interfacial hydrolysis and dissolution of silica. Therefore, the IL anion appears to influence the interfacial solvolysis mechanism and not necessarily the solubility of silica.

## 5.0. CONCLUSIONS

Mesoporous silica is thermochemically stable in anhydrous imidazolium-based ionic liquids. This ionothermal stability is quite different from its behavior in water where mesoporous silica degrades by hydrolytic depolymerization. Interestingly though, mesoporous silica is thermochemically stable in IL–water mixtures having water in amounts up to 75 mol %, whereas its dissolution is accelerated relative to water at finite IL compositions less than 15 mol %. We rationalize this composition-dependent solvothermal behavior of mesoporous silica as either because of the binary solvent solubility predicted by extended Hildebrand theory or solvent effects on the interfacial solvolysis rate. We postulate that the interfacial solvolysis mechanism is what dominates the dissolution process, and this is influenced by the solvent phase through adsorption of IL cations onto the silica surface. Additionally, by changing the identity of the IL anion, we find additional dissolution accelerations. These accelerations correlate with the aqueous phase nucleophilicity of the IL anions but inversely with their radius, supporting our hypothesis of cation adsorption. However, the solution pH is also found to depend similarly on the anion species and IL–water composition, suggesting indirect IL participation in the interfacial solvolysis mechanism. Nevertheless, this finding also supports the conclusion that the dissolution kinetics of mesoporous silica are controlled by interfacial solvolysis and not solubility. We therefore believe that the stability of mesoporous silica films against dissolution in anhydrous imidazolium ILs is principally due to their inability to hydrolytically depolymerize the silica matrix. Our findings then indicate that imidazolium ILs and certain compositional mixtures of these in water may be better solvents for a variety of applications involving mesoporous silica-based materials.

## ■ ASSOCIATED CONTENT

### Supporting Information

A complete description of the experimental methods; additional SEM, STEM, and r-SAXS data for the HTT, ITT, and HITT-BMIM-Cl treatments; RFT, RFRI, SEM, STEM, and r-SAXS data for the ITT- and HITT-BMIM-AcO, -Br, and -SCN treatments; and other pertinent experimental details and results. This material is available free of charge via the Internet at <http://pubs.acs.org>.

## ■ AUTHOR INFORMATION

### Corresponding Author

\*E-mail: daeyeon@seas.upenn.edu.

### Notes

The authors declare no competing financial interest.

## ■ ACKNOWLEDGMENTS

Our work was supported by NSF CBET-1033017, and J.H.P. acknowledges the support of an NSF-IGERT fellowship (DGE-0221664). The authors also acknowledge Prof. C. Kagan (University of Pennsylvania) for the use of the positive pressure glovebox; Prof. C. B. Murray (University of Pennsylvania) for allowing the use of the Rigaku SmartLab X-ray Intelligent Diffraction System; Dr. J. Ford (Penn Regional Nanotechnology Facility at University of Pennsylvania) for his guidance with STEM imaging; and Profs. R. J. Gorte (University of Pennsylvania), J. M. Vohs (University of Pennsylvania), and L. G. Sneddon (University of Pennsylvania) for their helpful discussions.

## ■ ABBREVIATIONS

BMIM	= 1-butyl-3-methylimidazolium
BMIM-AcO	= 1-butyl-3-methylimidazolium acetate
BMIM-Br	= 1-butyl-3-methylimidazolium bromide
BMIM-Cl	= 1-butyl-3-methylimidazolium chloride
BMIM-IL	= 1-butyl-3-methylimidazolium-based ionic liquid
BMIM-SCN	= 1-butyl-3-methylimidazolium thiocyanate
EISA	= evaporation-induced self-assembly
HTT	= hydrothermal treatment
HITT	= hydronothermal treatment
IL	= ionic liquid
ITT	= ionothermal treatment
MSF	= mesoporous silica film
PTFE	= polytetrafluoroethylene
r-SAXS	= reflectance-small-angle X-ray scattering
RFT	= relative film thickness
RFRI	= relative film refractive index
RI	= refractive index
SE	= spectroscopic ellipsometer or spectroscopic ellipsometry
SEM	= scanning electron microscopy
SGS	= silica sol–gel synthesis submixture
STEM	= scanning transmission electron microscopy
STS	= surfactant templating submixture
STT	= solvothermal treatment
TEM	= transmission electron microscopy

## ■ REFERENCES

- (1) Kresge, C. T.; Leonowicz, M. E.; Roth, W. J.; Vartuli, J. C.; Beck, J. S. Ordered Mesoporous Molecular Sieves Synthesized by a Liquid Crystal Template Mechanism. *Nature* **1992**, *359*, 710–712.
- (2) Raman, N. K.; Anderson, M. T.; Brinker, C. J. Template-Based Approaches to the Preparation of Amorphous, Nanoporous Silicas. *Chem. Mater.* **1996**, *8*, 1682–1701.
- (3) Asefa, T.; Tao, Z. Mesoporous Silica and Organosilica Materials — Review of their Synthesis and Organic Functionalization. *Can. J. Chem.* **2012**, *90*, 1015–1031.
- (4) Lu, A. H.; Schüth, F. Nanocasting: A Versatile Strategy for Creating Nanostructured Porous Materials. *Adv. Mater. (Weinheim, Ger.)* **2006**, *18*, 1793–1805.
- (5) Yang, P.; Zhao, D.; Margolese, D. I.; Chmelka, B. F.; Stucky, G. D. Block Copolymer Templating Syntheses of Mesoporous Metal

- Oxides with Large Ordering Lengths and Semicrystalline Framework. *Chem. Mater.* **1999**, *11*, 2813–2826.
- (6) Taguchi, A.; Schüth, F. Ordered Mesoporous Materials in Catalysis. *Microporous Mesoporous Mater.* **2005**, *77*, 1–45.
- (7) Shopsowitz, K. E.; Qi, H.; Hamad, W. Y.; MacLachlan, M. J. Free-Standing Mesoporous Silica Films with Tunable Chiral Nematic Structures. *Nature* **2010**, *468*, 422–426.
- (8) Khatib, S. J.; Oyama, S. T. Silica Membranes for Hydrogen Separation Prepared by Chemical Vapor Deposition (CVD). *Sep. Purif. Technol.* **2013**, *111*, 20–42.
- (9) Chew, T. L.; Ahmad, A. L.; Bhatia, S. Ordered Mesoporous Silica (OMS) as an Adsorbent and Membrane for Separation of Carbon Dioxide ( $\text{CO}_2$ ). *Adv. Colloid Interface Sci.* **2010**, *153*, 43–57.
- (10) Penard, A.-L.; Gacoin, T.; Boilot, J.-P. Functionalized Sol–Gel Coatings for Optical Applications. *Acc. Chem. Res.* **2007**, *40*, 895–902.
- (11) Afriyie, E. T.; Karami, P.; Norberg, P.; Gudmundsson, K. Textural and Thermal Conductivity Properties of a Low Density Mesoporous Silica Material. *Energy Buildings* **2014**, *75*, 210–215.
- (12) Galarneau, A.; Desplantier-Giscard, D.; Di Renzo, F.; Fajula, F. Thermal and Mechanical Stability of Micelle-Templated Silica Supports for Catalysis. *Catal. Today* **2001**, *68*, 191–200.
- (13) Azizi, S. N.; Ghasemi, S.; Yazdani-Sheldarrei, H. Synthesis of Mesoporous Silica (SBA-16) Nanoparticles using Silica Extracted from Stem Cane Ash and its Application in Electrocatalytic Oxidation of Methanol. *Int. J. Hydrogen Energy* **2013**, *38*, 12774–12785.
- (14) Zhao, D.; Huo, Q.; Feng, J.; Chmelka, B. F.; Stucky, G. D. Nonionic Triblock and Star Diblock Copolymer and Oligomeric Surfactant Syntheses of Highly Ordered, Hydrothermally Stable, Mesoporous Silica Structures. *J. Am. Chem. Soc.* **1998**, *120*, 6024–6036.
- (15) Lu, Y.; Ganguli, R.; Drewien, C. A.; Anderson, M. T.; Brinker, C. J.; Gong, W.; Guo, Y.; Soyez, H.; Dunn, B.; Huang, M. H.; Zink, J. I. Continuous Formation of Supported Cubic and Hexagonal Mesoporous Films by Sol–Gel Dip-Coating. *Nature* **1997**, *389*, 364–368.
- (16) Zhao, D.; Yang, P.; Melosh, N.; Feng, J.; Chmelka, B. F.; Stucky, G. D. Continuous Mesoporous Silica Films with Highly Ordered Large Pore Structures. *Adv. Mater. (Weinheim, Ger.)* **1998**, *10*, 1380–1385.
- (17) Vinu, A.; Hossain, K. Z.; Ariga, K. Recent Advances in Functionalization of Mesoporous Silica. *J. Nanosci. Nanotechnol.* **2005**, *5*, 347–371.
- (18) Swaddle, T. W.; Salerno, J.; Tregloan, P. A. Aqueous Aluminates, Silicates, and Aluminosilicates. *Chem. Soc. Rev.* **1994**, *23*, 319–325.
- (19) Meynen, V.; Cool, P.; Vansant, E. F. Verified Syntheses of Mesoporous Materials. *Microporous Mesoporous Mater.* **2009**, *125*, 170–223.
- (20) Alexander, G. B.; Heston, W. M.; Iler, R. K. The Solubility of Amorphous Silica in Water. *J. Phys. Chem.* **1954**, *58*, 453–455.
- (21) Rimer, J. D.; Trofymuk, O.; Navrotsky, A.; Lobo, R. F.; Vlachos, D. G. Kinetic and Thermodynamic Studies of Silica Nanoparticle Dissolution. *Chem. Mater.* **2007**, *19*, 4189–4197.
- (22) Ravenelle, R. M.; Schüffler, F.; D'Amico, A.; Danilina, N.; van Bokhoven, J. A.; Lercher, J. A.; Jones, C. W.; Sievers, C. Stability of Zeolites in Hot Liquid Water. *J. Phys. Chem. C* **2010**, *114*, 19582–19595.
- (23) Bootsma, J. A.; Shanks, B. H. Cellobiose Hydrolysis using Organic–Inorganic Hybrid Mesoporous Silica Catalysts. *Appl. Catal., A* **2007**, *327*, 44–51.
- (24) Olivier-Bourbigou, H.; Magna, L.; Morvan, D. Ionic Liquids and Catalysis: Recent Progress from Knowledge to Applications. *Appl. Catal., A* **2010**, *373*, 1–56.
- (25) Xinxin, H.; Armstrong, D. W. Ionic Liquids in Separations. *Acc. Chem. Res.* **2007**, *40*, 1079–1086.
- (26) Swatoski, R. P.; Spear, S. K.; Holbrey, J. D.; Rogers, R. D. Dissolution of Cellulose with Ionic Liquids. *J. Am. Chem. Soc.* **2002**, *124*, 4974–4975.
- (27) Mäki-Arvelaa, P.; Anugwoma, I.; Virtanena, P.; Sjöholm, R.; Mikkola, J. P. Dissolution of Lignocellulosic Materials and Its Constituents Using Ionic Liquids—A Review. *Ind. Crops Prod.* **2010**, *32*, 175–201.
- (28) Rinaldi, R.; Palkovits, R.; Schuth, F. Depolymerization of Cellulose Using Solid Catalysts in Ionic Liquids. *Angew. Chem., Int. Ed.* **2008**, *47*, 8047–8050.
- (29) Zhang, L.; Yu, H.; Wang, P. Solid Acids as Catalysts for the Conversion of D-Xylose, Xylan and Lignocellulosics into Furfural in Ionic Liquid. *Bioresour. Technol.* **2013**, *136*, 515–521.
- (30) Production of Biofuels and Chemicals with Ionic Liquids; Fang, Z., Ed.; Springer Science+Business Media: Dordrecht, The Netherlands, 2014; Vol. 1.
- (31) Huang, Y.-B.; Fu, Y. Hydrolysis of Cellulose to Glucose by Solid Acid Catalysts. *Green Chem.* **2013**, *15*, 1095–1111.
- (32) Rinaldi, R.; Meine, N.; vom Stein, J.; Palkovits, R.; Schuth, F. Which Controls the Depolymerization of Cellulose in Ionic Liquids: The Solid Acid Catalyst or Cellulose? *ChemSusChem* **2010**, *3*, 266–276.
- (33) Riisagera, A.; Fehrmanna, R.; Haumannb, M.; Wasserscheid, P. Supported Ionic Liquids: Versatile Reaction and Separation Media. *Top. Catal.* **2006**, *40*, 91–102.
- (34) Perdikaki, A. V.; Vangeli, O. C.; Karanikolos, G. N.; Stefanopoulos, K. L.; Beltsios, K. G.; Alexandridis, P.; Kanellopoulos, N. K.; Romanos, G. E. Ionic Liquid-Modified Porous Materials for Gas Separation and Heterogeneous Catalysis. *J. Phys. Chem. C* **2012**, *116*, 16398–16411.
- (35) Qian, X.; Lei, J.; Wickramasinghe, S. R. Novel Polymeric Solid Acid Catalysts for Cellulose Hydrolysis. *RSC Adv.* **2013**, *3*, 24280–24287.
- (36) Cai, H.; Li, C.; Wang, A.; Xu, G.; Zhang, T. Zeolite-Promoted Hydrolysis of Cellulose in Ionic Liquid, Insight into the Mutual Behavior of Zeolite, Cellulose and Ionic Liquid. *Appl. Catal., B* **2012**, *123–124*, 333–338.
- (37) Vangeli, O. C.; Romanos, G. E.; Beltsios, K. G.; Fokas, D.; Athanasekou, C. P.; Kanellopoulos, N. K. Development and Characterization of Chemically Stabilized Ionic Liquid Membranes—Part I: Nanoporous Ceramic Supports. *J. Membr. Sci.* **2010**, *365*, 366–377.
- (38) Vitz, J.; Erdmenger, T.; Haensch, C.; Schubert, U. S. Extended Dissolution Studies of Cellulose in Imidazolium Based Ionic Liquids. *Green Chem.* **2009**, *11*, 417–424.
- (39) Sievers, C.; Valenzuela-Olarte, M. B.; Marzialetti, T.; Musin, I.; Agrawal, P. K.; Jones, C. W. Ionic-Liquid-Phase Hydrolysis of Pine Wood. *Ind. Eng. Chem. Res.* **2009**, *48*, 1277–1286.
- (40) Marszall, M. P.; Kaliszak, R. Application of Ionic Liquids in Liquid Chromatography. *Crit. Rev. Anal. Chem.* **2007**, *37*, 127–140.
- (41) Rivera-Munoz, E. M.; Huirache-Acuna, R. Sol Gel-Derived SBA-16 Mesoporous Material. *Int. J. Mol. Sci.* **2010**, *11*, 3069–3086.
- (42) Voort, P. V. D.; Benjelloun, M.; Vansant, E. F. Rationalization of the Synthesis of SBA-16: Controlling the Micro- and Mesoporosity. *J. Phys. Chem. B* **2002**, *106*, 9027–9032.
- (43) Kim, T.-W.; Ryoo, R.; Kruk, M.; Gierszal, K. P.; Jaroniec, M.; Kamiya, S.; Terasaki, O. Tailoring the Pore Structure of SBA-16 Silica Molecular Sieve through the Use of Copolymer Blends and Control of Synthesis Temperature and Time. *J. Phys. Chem. B* **2004**, *108*, 11480–11489.
- (44) Dunphy, D. R.; Singer, S.; Cook, A. W.; Smarsly, B.; Doshi, D. A.; Brinker, C. J. Aqueous Stability of Mesoporous Silica Films Doped or Grafted with Aluminum Oxide. *Langmuir* **2003**, *19*, 10403–10408.
- (45) Bass, J. D.; Gross, D.; Boissiere, C.; Belamie, E.; Cordin, T.; Sanchez, C. Stability of Mesoporous Oxide and Mixed Metal Oxide Materials under Biologically Relevant Conditions. *Chem. Mater.* **2007**, *19*, 4349–4356.
- (46) Li, X.; Barua, S.; Rege, K.; Vogt, B. D. Tuning Stability of Mesoporous Silica Films under Biologically Relevant Conditions through Processing with Supercritical  $\text{CO}_2$ . *Langmuir* **2008**, *24*, 11935–11941.
- (47) Karout, A.; Pierre, A. Silica Gelation Catalysis by Ionic Liquids. *Catal. Commun.* **2009**, *10*, 359–361.

- (48) Zhang, Y.; Du, H.; Qian, X.; Chen, E. Y. X. Ionic Liquid–Water Mixtures: Enhanced  $K_w$  for Efficient Cellulosic Biomass Conversion. *Energy Fuels* **2010**, *24*, 2410–2417.
- (49) Szilagyi, I.; Szabo, T.; Desert, A.; Trefalt, G.; Oncsik, T.; Borkovec, M. Particle Aggregation Mechanisms in Ionic Liquids. *Phys. Chem. Chem. Phys.* **2014**, *16*, 9515–9524.
- (50) Fontecave, T.; Sanchez, C.; Azais, T.; Boissiere, C. Chemical Modification As a Versatile Tool for Tuning Stability of Silica Based Mesoporous Carriers in Biologically Relevant Conditions. *Chem. Mater.* **2012**, *24*, 4326–4336.
- (51) Mezger, M.; Schröder, H.; Reichert, H.; Schramm, S.; Okasinski, J. S.; Schöder, S.; Honkimäki, V.; Deutsch, M.; Ocko, B. M.; Ralston, J.; Rohwerder, M.; Stratmann, M.; Dosch, H. Molecular Layering of Fluorinated ILs at Charged (0001) Sapphire Surfaces. *Science* **2008**, *322*, 424–428.
- (52) Zhou, H.; Rouha, M.; Feng, G.; Lee, S. S.; Docherty, H.; Fenter, P.; Cummings, P. T.; Fulvio, P. F.; Dai, S.; McDonough, J.; Presser, V.; Gogotsi, Y. Nanoscale Perturbations of Room Temperature Ionic Liquid Structure at Charged and Uncharged Interfaces. *ACS Nano* **2012**, *6*, 9818–9827.
- (53) Lui, M. Y.; Crowhurst, L.; Hallett, J. P.; Hunt, P. A.; Niedermeyer, H.; Welton, T. Salts Dissolved in Salts: Ionic Liquid Mixtures. *Chem. Sci.* **2011**, *2*, 1491–1496.
- (54) Martin, A.; Wu, P. L.; Velasquez, T. J. Extended Hildebrand Solubility Approach: Sulfonamides in Binary and Ternary Solvents. *J. Pharm. Sci.* **1984**, *74*, 277–282.
- (55) Katayanagi, H.; Nishikawa, K.; Shimozaki, H.; Miki, K.; Westh, P.; Koga, Y. Mixing Schemes in Ionic Liquid-H<sub>2</sub>O Systems: A Thermodynamic Study. *J. Phys. Chem. B* **2004**, *108*, 19451–19457.
- (56) Gebbie, M. A.; Valtiner, M.; Banquy, X.; Fox, E. T.; Henderson, W. A.; Israelachvili, J. N. Ionic Liquids Behave as Dilute Electrolyte Solutions. *P. Natl. Acad. Sci. U.S.A.* **2013**, *110*, 9674–9679.
- (57) Łuczak, J.; Hupka, J.; Thöming, J.; Jungnickel, C. Self-Organization of Imidazolium Ionic Liquids in Aqueous Solution. *Colloids Surf., A* **2008**, *329*, 125–133.
- (58) Reinert, L.; Batouche, K.; Lévéque, J.-M.; Muller, F.; Bény, J.-M.; Kebabi, B.; Duclaux, L. Adsorption of Imidazolium and Pyridinium Ionic Liquids onto Montmorillonite: Characterisation and Thermodynamic Calculations. *Chem. Eng. J. (Amsterdam, Neth.)* **2012**, *209*, 13–19.
- (59) Dove, P. M.; Nix, C. J. The Influence of the Alkaline Earth Cations, Magnesium, Calcium, and Barium on the Dissolution Kinetics of Quartz. *Geochim. Cosmochim. Acta* **1997**, *61*, 3329–3340.
- (60) Bai, S.; Urabe, S.; Okaue, Y.; Yokoyama, T. Acceleration Effect of Sulfate Ion on the Dissolution of Amorphous Silica. *J. Colloid Interface Sci.* **2009**, *331*, 551–554.
- (61) Marszall, M. P.; Baczek, T.; Kaliszan, R. Evaluation of the Silanol-Suppressing Potency of Ionic Liquids. *J. Sep. Sci.* **2006**, *29*, 1138–1145.
- (62) Zapata, P. A.; Faria, J.; Ruiz, M. P.; Jentoft, R. E.; Resasco, D. E. Hydrophobic Zeolites for Biofuel Upgrading Reactions at the Liquid-Liquid Interface in Water/Oil Emulsions. *J. Am. Chem. Soc.* **2012**, *134*, 8570–8578.
- (63) Swain, C. G.; Scott, C. B. Quantitative Correlation of Relative Rates. Comparison of Hydroxide Ion with Other Nucleophilic Reagents toward Alkyl Halides, Esters, Epoxides and Acyl Halides. *J. Am. Chem. Soc.* **1953**, *75*, 141–147.
- (64) Marcus, Y. A Simple Empirical Model Describing the Thermodynamics of Hydration of Ions of Widely Varying Charges, Sizes, and Shapes. *Biophys. Chem.* **1994**, *51*, 111–127.
- (65) Handy, S. T.; Okello, M. The 2 Position of Imidazolium Ionic Liquids: Substitution and Exchange. *J. Org. Chem.* **2005**, *70*, 1915–1918.
- (66) Momeni, M. R.; Rivard, E.; Brown, A. Carbene-Bound Borane and Silane Adducts: A Comprehensive DFT Study on Their Stability and Propensity for Hydride-Mediated Ring Expansion. *Organometallics* **2013**, *32*, 6201–6208.
- (67) Mazer, J. J.; Walther, J. V. Dissolution Kinetics of Silica Glass as a Function of pH Between 40 and 85°C. *J. Non-Cryst. Solids* **1994**, *170*, 32–45.
- (68) Dietzel, M. Dissolution of Silicates and the Stability of Polysilicic Acid. *Geochim. Cosmochim. Acta* **1999**, *64*, 3275–3281.
- (69) Pham, A. L.-T.; Sedlak, D. L.; Doyle, F. M. Dissolution of Mesoporous Silica Supports in Aqueous Solutions: Implications for Mesoporous Silica-Based Water Treatment Processes. *Appl. Catal., B* **2012**, *126*, 258–264.